Remote Sens. **2014**, *6*, 11915-11935; doi:10.3390/rs61211915

OPEN ACCESS

remote sensing

ISSN 2072-4292

www.mdpi.com/journal/remotesensing

Article

Quantitative Analysis of VIIRS DNB Nightlight Point Source for Light Power Estimation and Stability Monitoring

Changyong Cao [1,*] and Yan Bai [2]

[1] NOAA (National Oceanic and Atmospheric Administration)/NESDIS (National Environmental Satellite, Data, and Information Service)/STAR (Center for Satellite Applications and Research), NCWCP, E/RA2, 5830 University Research Ct., Suite 2838, College Park, MD 20740, USA

[2] CICS(Cooperative Institute for Climate and Satellites), ESSC Building, RM3250, University of Maryland, 5825 University Research Ct. College Park, MD 20740, USA; E-Mail: Yan.Bai@noaa.gov

* Author to whom correspondence should be addressed; E-Mail: Changyong.Cao@noaa.gov; Tel.: +1-301-683-3600; Fax: +1-301-683-3616.

External Editors: Christopher D. Elvidge and Prasad S. Thenkabail

Received: 10 September 2014; in revised form: 18 November 2014 / Accepted: 18 November 2014 / Published: 1 December 2014

Abstract: The high sensitivity and advanced onboard calibration on the Visible Infrared Imaging Radiometer Suite (VIIRS) Day/Night Band (DNB) enables accurate measurements of low light radiances which leads to enhanced quantitative applications at night. The finer spatial resolution of DNB also allows users to examine social economic activities at urban scales. Given the growing interest in the use of the DNB data, there is a pressing need for better understanding of the calibration stability and absolute accuracy of the DNB at low radiances. The low light calibration accuracy was previously estimated at a moderate 15% using extended sources while the long-term stability has yet to be characterized. There are also several science related questions to be answered, for example, how the Earth's atmosphere and surface variability contribute to the stability of the DNB measured radiances; how to separate them from instrument calibration stability; whether or not SI (International System of Units) traceable active light sources can be designed and installed at selected sites to monitor the calibration stability, radiometric and geolocation accuracy, and point spread functions of the DNB; furthermore, whether or not such active light sources can be used for detecting environmental changes, such as aerosols. This paper explores the quantitative analysis of nightlight point sources, such as those from fishing

vessels, bridges, and cities, using fundamental radiometry and radiative transfer, which would be useful for a number of applications including search and rescue in severe weather events, as well as calibration/validation of the DNB. Time series of the bridge light data are used to assess the stability of the light measurements and the calibration of VIIRS DNB. It was found that the light radiant power computed from the VIIRS DNB data matched relatively well with independent assessments based on the *in situ* light installations, although estimates have to be made due to limited ground truth data and lack of suitable radiative transfer models. Results from time series analysis are encouraging in potentially being able to detect anomalies in the DNB calibration. The study also suggests that accurate ground based active lights, when properly designed and installed, can be used to monitor the stability of the VIIRS DNB calibration at near the specified minimum radiances (3 $nW \cdot cm^{-2} \cdot sr^{-1}$), and potentially can be used to monitor the environmental changes as well.

Keywords: Suomi NPP; VIIRS; DNB; nightlight; bridge; calibration/validation; accuracy; stability; point source

1. Introduction

Among the twenty-two bands of the Visible Infrared Imaging Radiometer Suite) (VIIRS) onboard the Suomi National Polar-orbiting Partnership (NPP) satellite, the Day/Night Band (DNB) represents an unprecedented night observation capability. It is superior to its predecessor Operational Line Scanner (OLS) on the Defense Meteorological Satellite Program (DMSP) in both spatial and radiometric performance because it has a finer spatial resolution of constant 742 m across the three thousand kilometer scan, while for the first time it is calibrated using the onboard solar diffuser. The dynamic range of the DNB spans seven orders of magnitude from bright day light to the faint light of air glows, achieved with a three gain stage design: the low gain for high radiances at day time, the high gain for low radiances at night time, and the medium gain for radiances between day and night [1–3]. Although the specified radiance dynamic range is between 3×10^{-9} $W \cdot cm^{-2} \cdot sr^{-1}$ to 0.02 $W \cdot cm^{-2} \cdot sr^{-1}$, the VIIRS DNB on-orbit actually significantly outperforms the instrument specification at low light with a noise floor at about 5×10^{-11} $W \cdot cm^{-2} \cdot sr^{-1}$ [1–3]. The onboard calibration uses the solar diffuser to determine the low gain, which is then transferred to the mid and high gain stages using gain ratios determined near the terminator transient zones where all three gain stages have valid values. The radiometric accuracy of the high gain was estimated at about 15% in one study, while for the low gain stage, it is comparable to that of the VIIRS RSB band, which is at 2% [3,4]. There is a desire to improve the calibration accuracy and stability at low radiances to support novel low light applications, especially given the movement towards low nightlight for energy savings in lighting requirements, which will likely lead to lower radiances at night in the future worldwide.

The VIIRS DNB produces panchromatic imagery (0.5 to 0.9 μm) of the Earth in daytime, and at night with moonlight up to half illuminated lunar disk. The constant pixel size across scan is achieved in 32 aggregation zones, with 16 pixels per scan aggregated from 672 detectors in the track direction.

Many applications have been developed since the Suomi NPP launch to use the DNB data qualitatively in the form of light maps to examine the geospatial patterns. Limited applications also take advantage of the quantitative values of radiance in aggregated form by geographic regions [5]. However, previous studies are often limited by the traditional qualitative image display and aggregated regional statistical analysis methods used, which often obscures the underlining features or processes at the pixel-level for which point source analysis is essential. A better understanding of the active nightlight point sources will potentially open up new opportunities for more quantitative applications of the DNB, including object tracking, and stability monitoring of both the instrument and the environment.

It should be noted that a stable light database is currently being developed at the National Oceanic and Atmospheric Administration (NOAA) National Geophysical Data Center (NGDC) and a limited number of data sets are already made available to users [6,7], However, the NGDC dataset is a monthly mean composite of the stable lights by averaging pixels in clear sky observations in 15 arc second grids spanning 65 south to 75 north latitude. In the current study, the original measurements, instead of averaged values, are needed to study the stability of the nightlight observations at pixel-level because the averaging of radiances unfortunately removes the signal for our stability study. We study the DNB night radiances at the pixel-level for selected targets and sites in radiometric three-dimensional space where the radiances are used as Z values at each latitude and longitude location. The radiant power and electrical power of the lights are estimated using fundamental radiometry for the point sources to cross validate the DNB observations. The stability of night lights over time for these sites is analyzed using time series data. Factors affecting nightlight stability are investigated in terms of atmospheric effects, surface reflectance, light source stability, and geometric factors. The suitability of physical models in atmospheric radiative transfer for quantifying these environmental effects is also explored.

In the following, Section 2 introduces the methodology used in our study, Section 3 describes the data sets, and Section 4 presents the results and discussion. Conclusions are provided in the final section.

2. Methodology

Three methods are used in the data analysis in this study: the fundamental radiometry method is used to compute the radiant power based on the radiance, geometric factors, and sensor spectral response, as well as point spread functions, which allows us to further assess the electric power used; the 3D analysis of the point source radiance data using the point cloud method greatly facilitated the quantitative analysis of the data; and the radiative transfer models allow us to estimate the light transmission through the atmosphere and reflection from surfaces.

2.1. Fundamental Radiometry Equations and Scenarios for DNB Nightlight Applications

The primary equation used for computing the radiant power is:

$$\Phi = \frac{L}{\tau} \cdot \mathrm{dA} \cdot \cos\theta \mathrm{d}\Omega \tag{1}$$

where Φ = in-band radiant exitance from the target (watts); L = in-band radiance at the satellite sensor VIIRS DNB ($W \cdot cm^{-2} \cdot sr^{-1}$); Ω = projected solid angle in sr; θ = angle between the area surface normal

and the line of observation; τ = atmospheric transmittance (scattering is neglected in this study as discussed later); dA = area in m^2 (dA cosθ gives the projected area).

With the following additional constrains:

(1) Small angle approximation in which distance of the observer >> A

(2) On-axis (or nadir view) cosθ = 1

(3) Lambertian source with a size << pixel size.

Equation (1) can be reduced to Equation (2) below:

$$\Phi = \frac{L}{\tau} \cdot A \cdot \Omega \tag{2}$$

In this study, Equation (2) is used for calculating the radiant power from the DNB pixel given the radiance values. In this case the L is obtained from the VIIRS DNB radiance in the unit of $W \cdot cm^{-2} \cdot sr^{-1}$; A is the area of the pixel which is 742 × 742 square meters; Ω as a projected solid angle is nominally π for a Lambertian surface. τ is calculated from MODTRAN for a given atmosphere, and cross checked using NASA AERONET AOT values whenever available.

To estimate the electrical power used (P_e) for a point source, such as a light bulb, radiating into a solid angle (Ω_p) with a radiant to electrical power efficacy of ε, and illuminating a surface such as the ground with a Lambertian reflectance of ρ, we use the following equation:

$$P_e = \frac{\Phi}{\varepsilon \cdot \rho} \cdot \frac{\Omega_p}{\omega} \tag{3}$$

where ω is the effective solid angle intercepted by the area of the illuminated surface, which can be computed based on the lamp height, and the spherical cap of the area illuminated [8]. In addition, note that Ω_p is nominally 2π for a streetlight, while it is smaller for a spotlight or flood-lamp. It should be noted that Φ is the radiance power within the spectral response range of the VIIRS DNB.

Equations (2) and (3) are applicable to a typical scenario of nightlight observation from VIIRS DNB as described below (Figure 1). Given an active light source such as a light bulb illuminating the surface, e.g., a parking lot, bridge, or the deck of a boat, the light is reflected by the surface and then propagated through the atmosphere, subjected to atmospheric transmission and molecular/aerosol scattering before it reaches the satellite sensor VIIRS DNB. Only photons within the bandpass of the DNB can be detected, which is manifested in the radiance unit ($W \cdot cm^{-2} \cdot sr^{-1}$) as integrated power over the entire spectral response range of the DNB (Figure 2). Note that a significant portion (on the order of 34%) of the radiant power from the white Light Emitting Diode (LED) is not captured by the DNB because the blue "pump" (peak near 450 nm) of the white LED is out of the spectral response of the DNB. By comparison, the High Pressure Sodium (HPS) spectra is mostly within the DNB spectral response range (Figure 2). This issue is further discussed later in the validation of DNB radiances.

The focus of this study is on the active nightlights at pixel-level, which can be originated from city streets, bridges, airports, or ships. The typical active light source is a point source, which is a single identifiable localized source of light. A point source has negligible extent relative to the distance to the observer, distinguishing it from extended source. This facilitates modeling and analysis since the light source can be approximated as a mathematical point. It should be noted that in VIIRS DNB

observations, multiple point sources may contribute to the radiances at pixel-level (with an area of 742 m × 742 m).

Figure 1. Nightlight Propagation.

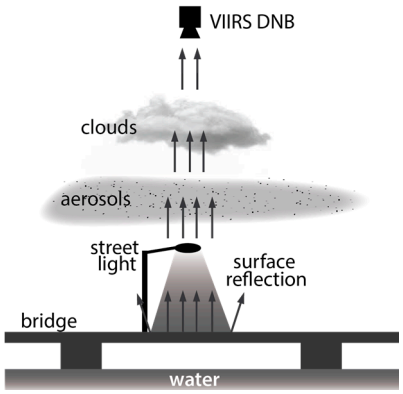

Figure 2. VIIRS DNB relative spectral response (RSR) function.

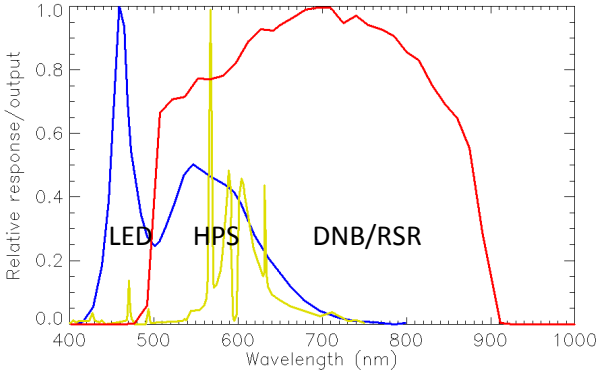

Background shows typical LED and High Pressure Sodium (HPS) Lamp Spectrum.

The point source needs to be convolved with the spatial response of the VIIRS DNB or the line spread function (LSF), both along- and cross-track. Along-track, the LSF is known to be a rectangular function. However, with cross-track, the VIIRS DNB LSF is rather complex due to the 32 aggregation zones and each zone has a slightly different LSF. To simplify the calculations, in this study we only consider the near nadir observations in aggregation zone 1, which has an approximately rectangular cross-track LSF (Figure 3) [9].

It is known that for the low light measurements (in high gain stage), the VIIRS DNB design is rather sophisticated, consisting of two redundant Charge-Coupled Device (CCD) arrays, each with 250 × 672 subpixles. The 250 subpixels in the scan direction allows the repeated measurements of the same target with time delay integration (TDI) to achieve a high signal to noise ratio. Spatially, the subpixels are aggregated in both the scan and track directions according to a complex scheme to achieve the near constant resolution of 742 × 742 meters across scan and along track. In this study, we focus on the DNB measurements at the pixel-level near nadir without involving discussions of the subpixel or CCD level [10].

Figure 3. DNB Line Spread Function (LSF) along scan. Agg zone 1 is used in this study to avoid complex LSF effects [9].

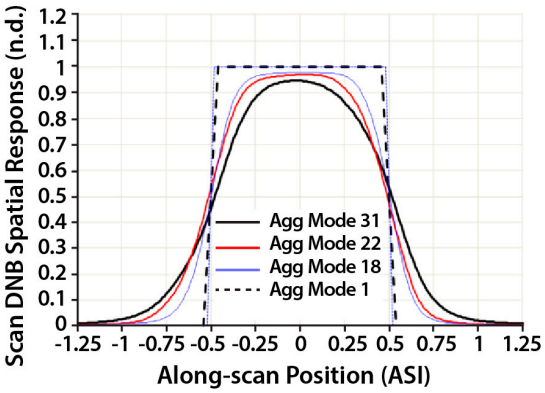

2.2. Point Cloud Analysis

In typical two-dimensional image analysis, the radiance for each pixel is represented as a dot on the computer screen with brightness scaled between 0 and 255. In the onscreen analysis, the radiometric values are significantly dithered or quantized especially for the DNB data, which has a dynamic range several orders of magnitude. This obscures the true radiances in the DNB nightlight data. When the pixels with high values are displayed clearly by changing the display range, the pixels with low values become too dark to be seen. While when the low values are enhanced on the screen, the pixels with high values are over-saturated. This problem is alleviated in radiometric 3D analysis because the vertical axis in such analysis represents the absolute radiometric quantity at each latitude longitude.

Although three-dimensional analysis is not new, its applications to DNB data analysis are significantly hindered by the capabilities in popular software packages. There are several issues. First, the DNB data at pixel-level often appear in the form of point source or impulses, which is fundamentally different from 3D terrain models that have a much lower spatial frequency. As a result, most Earth science software packages have difficulty in creating 3D models from the DNB data. Another problem is that the numerical values in DNB at night are extremely small (on the order of 10^{-9}) and at least some popular commercial software packages are unable to display the values correctly. In this study we use a procedure to convert the DNB data to point cloud and then 3D models, which can be viewed and analyzed in popular 3D software packages. Three-dimensional mesh can also be created for display, and can even be realized in solid 3D form by 3D printing if so desired to facilitate the analysis and comparisons (Figure 4). As the radiometric Z values are preserved as they are measured in the original data, this makes it comparable not only between geographical areas, such as between cities, but also temporally, allowing us to study nightlight stability effectively and quantitatively.

Figure 4. Comparison of 3D (**left**) *versus* 2D (**right**) view of the VIIRS DNB nightlight for Geneva, Switzerland.

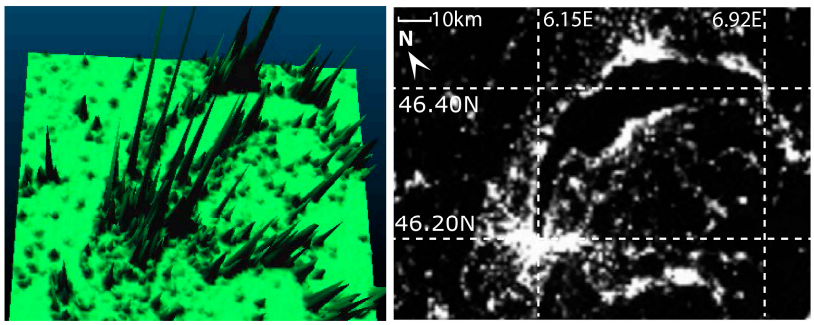

The point cloud method is relatively straightforward (note that the "cloud" here is considered part of cloud computing and is not directly related to the physical "cloud"). VIIRS DNB data for selected sites are obtained from the NOAA CLASS archive. For each site, the DNB data are converted to point cloud, which is essentially latitude, longitude, radiance values as x, y, and z. The radiance value for each pixel is also used as the attribute (or named scaler in some 3D software packages) for analysis. If the satellite projection instead of lat/lon projection is preferred, the lat/lon values are replaced by position index of the pixel for the dataset. The Point cloud datasets are analyzed using the CloudCompare in this study, which is an open source software package originally designed for 3D point cloud processing and is especially suitable for comparisons between datasets [11], and for picking particular points for analysis. The following are detailed steps.

(1) From radiance to point clouds: In this study, the radiometric values are used as the vertical axis for the point clouds which forms the radiometric 3D models of the DNB. Given the VIIRS DNB radiance unit of $W \cdot cm^{-2} \cdot sr^{-1}$, the typical night light radiances have values between 1.0–300 × 10^9 $W \cdot cm^{-2} \cdot sr^{-1}$. To facilitate analysis, we use the unit of $nW \cdot cm^{-2} \cdot sr^{-1}$ by multiplying 10^9, which makes the radiance values more manageable. This unit is interchangeably used with 10^{-5} $W \cdot m^{-2} \cdot sr^{-1}$, which is preferred in cases where meters are used.

(2) Geospatial matching between VIIRS DNB observations. The point cloud method allows the original data in lat/lon and radiance to be preserved in the processing and comparisons. In traditional image comparisons, both images would have to be re-projected to a common map projection or grid in order for them to match spatially pixel-by-pixel. However, re-projection may change the pixel values or change the pixel shape/size, which is not desirable for this study. Therefore, point clouds have unique advantages in this analysis because it allows the comparison of observations from different time periods for the same latitude/longitude location to evaluate the nightlight stability at the site. In matching the data points between DNB observations, we used the lat/lon information for each point to find the nearest neighbor point since their precise locations on the image may not be identical between observations.

(3) Identification of features. Nightlight images are made of pixels with different radiance values. Using the "point picking" feature in CloudCompare, a point of interest can be identified from the point cloud dataset with latitude and longitude values. The lat/lon values are then used to identify the geographic feature using the Google map. The radiometric value of the selected point is also readily available.

(4) Differencing between datasets. Datasets for the same site but different times are compared in point cloud analysis. Two methods are used: one is to compare datasets from two different times of observations to assess the radiance differences at selected pixels; two is to combine all points from different times into one dataset with different layers to identify points that are stable. Temporal data with bright and stable nightlights should form clusters in the point clouds and easily identifiable in the analysis.

2.3. Candidate Radiative Transfer Models for DNB

It is known that the atmosphere plays an important role in the stability of the nightlights observed by the VIIRS DNB. To estimate the effects due to various atmospheric conditions, physical models of the light propagation need to be used. Several radiative transfer models have been developed by various communities. Here we review two groups: one from the astronomy and army community for the study of light pollution and urban illumination, including the AAIM (An Army Illumination Model) and LPTRAN (Light Pollution Radiative Transfer); and the other from the remote sensing and atmospheric science, which includes MODerate resolution atmospheric TRANsmission (MODTRAN), Second Simulation of a Satellite Signal in the Solar Spectrum (6S), and Community Radiative Transfer Model (CRTM). These models are evaluated for fitness and suitability for the light propagation through the atmosphere to account for the variability of the light intensity between observations in VIIRS DNB. The model choices and limitations are discussed below.

The Garstang model [12] is commonly used by the astronomy community and it estimates city brightness as a function of distance, look-angle, city population, and atmospheric clarity. It uses radiative transfer approximations including first and second order Rayleigh and aerosol scattering, and ground albedo, curvature of the earth's surface, and the areal distribution of the light source to calculate the sky light intensity. This model assumes that the city lighting produces an output represented as lumens per head of population, a fraction of which is radiated directly into the upper hemisphere. Although the Garstang model considers the physical process of light propagation through the atmosphere and surfaces, it treats an entire city as one circular object. The light intensity is empirically derived based on population and other social economic parameters, and therefore it lacks the spatial resolution and physical basis for pixel-level light intensity analysis intended for this study. In particular, the Garstang model would not be useful for the atmospheric correction of the DNB observations.

The Garstang model has several derivatives for different applications. One of which is the An Army Illumination Model (AAIM) [13]—A highly simplified and parameterized version of Garstang's model with extensions to include cloudy skies and lunar illumination. In AAIM, the observer is located at ground level. This model was developed to predict broadband brightness as a function of population and distance (>10 km) from city center under clear and overcast conditions. It provides illumination levels for cities for use with Night Vision Goggles. It may be used in tactical decision aids and war-games for an observer at ground level, allowing for more accurate prediction of target acquisition ranges and increased realism in simulations.

The LPTRAN [14] is considered an extended Garstang model for DMSP-OLS radiance measurements, which also incorporates digital elevation data. It can be used to predict the artificial

brightness distribution of the night sky at a site in the world at visible wavelength for a broad range of atmospheric situations and the artificial radiation density in atmosphere across the territory. This model is mostly used to address the increasing concern with the problem of light pollution in the astronomical community.

While the Garstang and derivative models are developed specifically for the propagation of city lights with very low spatial resolution, many generic atmospheric radiative transfer models (RTM) have been developed and refined in the past decade based on first principles physics. In the visible and near infrared spectrum, the RTMs are developed for solar and lunar light propagation through the atmosphere and surface for computing the satellite at sensor radiances. The model calculates radiative transfer of electromagnetic radiation through the Earth's atmosphere. It relies on the radiative transfer equation that is numerically solved using a solver such as a discrete ordinate method. The radiative transfer equation is a monochromatic equation to calculate radiance in a single layer of the Earth's atmosphere. The calculation involves the spectral convolution of the atmospheric spectrum with the instrument spectral response functions, which may require line-by-line calculations for all molecules in the atmospheric layer. Alternatively, a set of pre-calculated coefficients can be prepared for band transmission for faster calculations. In addition, models may consider scattering from molecules or particles, as well as polarization.

Popular radiative transfer models include the MODTRAN, 6S, and CRTM. MODTRAN [15] is designed to model atmospheric propagation of electromagnetic radiation for the 0.2 to 100 μm spectral range, which covers the spectrum from middle ultraviolet to visible light to far infrared. It can be run in either atmospheric transmittance or both atmospheric transmittance and radiance mode for any given slant path geometry under either solar or lunar illuminations in the visible to near infrared. Although MODTRAN is versatile in defining observation geometries, the irradiance source is limited to either the sun or the moon, and does not offer the option to include artificial sources near the surface, as is needed in our study for VIIRS DNB nightlight. On the other hand, the atmospheric transmittance can be computed from the ground to satellite path, which is useful for estimating the absorption along the path of nightlights.

6S (Second Simulation of a Satellite Signal in the Solar Spectrum) was developed to simulate the reflection of solar radiation by a coupled atmosphere-surface system for a wide range of atmospheric, spectral and geometrical conditions [16]. It was designed to perform atmospheric correction for the process of removing the effects of the atmosphere on the reflectance values of images taken by satellite or airborne sensors. The code operates on the basis of an SOS (successive orders of scattering) method and the vector version 6SV accounts for the polarization of radiation in the atmosphere through the calculation of the Q and U components of the Stokes vector. It has been used for the calculation of look-up tables in the MODIS atmospheric correction algorithm. However, similar to MODTRAN, the source used for 6S is the solar spectrum and does not have provision for artificial light sources. On the other hand, the atmospheric effects covered in the 6S spectral range is sufficient for the DNB applications. This also reduces the complexity of the code, which is an advantage when modification is needed for DNB applications. The model is well documented in journal publications, which makes it relatively straight forward to be adapted for DNB nightlight applications.

Community Radiative Transfer Model [17] is a fast radiative transfer model for calculations of radiances for satellite visible-near-infrared, infrared or microwave radiometers. Given an atmospheric

profile of temperature, variable gas concentrations, cloud and surface properties, CRTM calculates radiances and brightness temperatures at the satellite sensor. CRTM contains forward, tangent linear, adjoint and K (full Jacobian matrices) versions of the model, with the latter three modules for variational assimilation or retrieval applications. CRTM has been improved significantly in recent years and has been used in the satellite data assimilation for numerical weather forecast operationally. The source code for CRTM is readily available. However, unlike the other radiative transfer models where users can define the sensor spectral response functions, CRTM only supports sensors that are already included in the code because it relies on a set of pre-calculated coefficients for a given sensor for fast calculations. For any new sensor band such as the VIIRS DNB, users will need to request the sensor to be included in the model before it can be used [18].

Although most of the radiative transfer codes discussed here have the potential to be used for calculating night artificial light propagation up to the satellite sensor, none of them can be readily used as is because artificial light source was not in any of the design considerations and changes will have to be made to the code to do so. As a result, none of the models can be used to fully calculate the radiative transfer of nightlights. Instead, this study is limited to the experimentation with atmospheric transmittance calculations of the nightlight, which is accomplished with MODTRAN. The atmospheric transmittance for the DNB is computed by varying the amount of water vapor, aerosol, and other parameters to estimate the effect on the light stability. Radiative transfer calculations of scattering for artificial nightlight as point sources can be difficult with existing models and, therefore, will require further work in the near future.

3. Data Sets Used in This Study

There are several considerations in selecting the datasets for this study. First, the integrated radiance within the 742 × 742 pixel needs to be above the VIIRS DNB specified minimum detectable radiance L_{min} (3 $nW \cdot cm^{-2} \cdot sr^{-1}$). Second, the pixel radiance value should not be contaminated by neighboring pixels. Ideal scenarios would a point source with a complete dark background, such as an isolated fishing boat in the ocean during new moon. Third, the number of light bulbs within the pixel can be accurately counted. This is easily achievable if the number of light bulbs within a pixel is small, or they are equally spaced spatially, such as those on bridges. This will allow the validation of such light sources. Other desirable requirements include the stability of the lights, and low variability in the environmental factors, such as aerosol, cloud, and water vapor. Apparently, not all requirements can be easily met. In this study, we identified selected fishing vessels, bridges, and city lights for analysis. Their advantages and limitations are investigated.

3.1. DNB Data for the Alaska Crab Fishing Vessel Rescue

It was reported that VIIRS DNB data was used to help an Alaska crab-fishing vessel trapped in sea ice in the Bearing Sea on 13 February 2013 (~14:22Z), to navigate through and out of the sea ice that was reaching one meter in thickness. The light from the boat was clearly seen from the DNB imagery [19], which helped plotting a rescue route avoiding thicker ice. This DNB dataset provides a good example of DNB response to a point source and therefore is used in our analysis. This particular data set was taken near new moon (with 12% lunar disk illumination). Therefore, the background in

this dataset shows negligible reflected lunar light from the sea and ice. However, limited information about the vessel is publicly available since it is privately owned.

3.2. DNB Time Series Data for the San Mateo and Incheon Bridges

Bridges provide a good nightlight point source because the light illumination is typically reflected from the concrete road surface, while the water below it has low reflection. Lights on the bridge are expected to be relatively stable both in geolocation and light intensity. However, not all bridge lighting is suitable for DNB studies. For example, we found that the lights on the Chesapeake Bay bridge near Annapolis, MD, and the Lake Pontchartrain Bridge are too dark to be seen by the DNB. On the other hand, lights on the San Mateo bridge and the Incheon Airport bridge are above the minimum radiance specification (L_{min}) and therefore the data are used for analysis in this study with one year of time series for each bridge. The sampling interval is every 16 days following the orbital repeat cycle in order to get VIIRS DNB data with near identical view geometry for the time series.

3.3. DNB Data for Geneva, Switzerland

This dataset is mainly used to assess the stability of the brightest lights in the city, since lights at other intensities are typically mixed with nearby sources in the city. With a population of about 184 thousand, Geneva is a relatively small city in Europe known as homes for dozens of international organizations. Geneva is chosen for this study because its size is relatively small and the city is well known internationally. The Geneva lake can be used as a dark background for the DNB nightlight for comparisons.

4. Results and Discussion

4.1. Point Source Data Analysis

From the Bearing Sea crab-fishing vessel dataset, we found that although the vessel itself (about 34 meters × 10.4 meters) is much smaller than one VIIRS DNB pixel, there are actually 24 pixels illuminated in the DNB for this vessel, with a Gaussian like distribution (Figure 5; Table 1), and a maximum pixel radiance value of 3.652 $nW \cdot cm^{-2} \cdot sr^{-1}$, which is at the level of specified minimum radiance for the VIIRS DNB instrument. Since the actual DNB minimum detectable radiance is more than an order of magnitude smaller and the background ocean has little light, the vessel signal is clearly detected. This is very significant for search and rescue operations where the light intensity of the object is usually relatively small. The multiple pixel illumination could have been mis-interpreted as a point spread effect of the instrument, but this is not possible since the resolution of the instrument is 742 meters at full-width-half-max (FWHM), and as discussed later, there are indeed single points illuminated in the DNB datasets such as shown in other datasets for both fishing boats and city lights.

Figure 5. 3D view of the Bearing Sea crab vessel light (in satellite projection to avoid distortion).

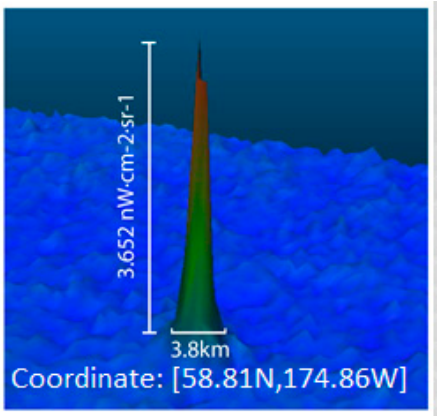

Table 1. Radiant Power Calculation for the Crab Fishing Vessel.

	Value	Note
Total Radiance	29.62 $nW \cdot cm^{-2} \cdot sr^{-1}$	
# of illuminated pixels	24	
Atmospheric transmittance [1]	95%	MODTRAN estimates
Radiant exitance	171.65 $W \cdot sr^{-1}$	Equation (1)
Surface Lambertian reflection	50%	Assumption
Total irradiance incident on surface	1078.5W	Equations (1) and (2)
Lamp electrical to Radiant Power conversion efficacy	30%	Assume HPS; would be much higher for Tungsten
Estimated total electrical power used	3.6kW	

[1] Based on MODTRAN and AERONET.

Since the vessel is not located near nadir on the DNB image, one possibility for the multiple pixel illumination is that the vessel light is in the corner of four DNB pixels which would illuminate about 8 pixels (worst case scenario) since the LSF along scan is responsive to ±1.25 pixels while a rectangular response is assumed in the track direction (Figure 3). However, the 24 pixel illumination far exceeded the effect of the LSF and as a result, the alternative explanation is that a combination of near field scattering in the DNB instrument, and light scattering in the clouds have likely contributed to the illumination of a much large area. The symmetric pattern of the illuminated pixels also supports the hypothesis of scattering, since the LSF is not symmetric in the track and scan directions. To further verify this assumption, we analyzed the cloud optical thickness data for this granule [20,21]. The data shows that a mixture of ice and water clouds dominated the region at the time of DNB observation, which supports the hypothesis of cloud scattering. It is also possible that scattering would be different in water clouds *vs.* ice clouds, which will require further analysis in the future. Another possible explanation is that there may have been multiple vessels at this location and time. However, detecting individual vessels within a group of contiguously illuminated pixels at 742 m resolution exceeded the spatial performance limit of the DNB. In addition, the ground truth data is not available in this case.

Finally, it should be noted that the VIIRS DNB LSF on-orbit has not been fully verified. Additional work is also needed to derive a more solid LSF in both the scan and track directions.

Analysis of the light intensity of the fleet near the St. Paul Island (southeast of the trapped vessel) shows that there were many vessels in the area at the time, some with a similar level of radiance values with multiple pixel illumination, although vessels with radiances as low as 0.987 $nW \cdot cm^{-2} \cdot sr^{-1}$ with a single pixel illumination have also been detected. This compares to a background radiance of ~0.2 $nW \cdot cm^{-2} \cdot sr^{-1}$ which is for the ocean surface.

To estimate the light power from the fishing vessel, Equation (1) is used. Given the total radiance of the 24 pixels illuminated, we derive the radiant exitance of 171.65 $W \cdot sr^{-1}$. We further assume that the vessel surface has a reflection of 50% (possibly higher if there is snow), and the lamp used is assumed to be High Pressure Sodium (HPS) floodlights [22], which have a 30% electrical to radiant conversion efficacy. The estimated total electrical power required would be about 3.6 kW. Alternatively, if the lamp type is Halogen-Tungsten, the electric power required could be lower because of its higher efficacy. It is noted that the floodlights in this case would be primarily used to illuminate the deck of the vessel for operations, in contrast to the squid fishing boats where the light is primarily used for attracting the fish. For comparison, we also analyzed sample lights for squid fishing boats in the Sea of Japan, which suggests that the light power (typically >130 $nW \cdot cm^{-2} \cdot sr^{-1}$) is many times higher than that of the crab fishing vessel analyzed here. This demonstrates that the light power calculations can potentially be used to obtain more information about the vessels and objects of interest.

The vessel lights have strong signals for DNB and are very useful for tracking and identification, but unfortunately, they are mobile and therefore not suitable for long-term stability analysis for obvious reasons. Therefore, for long-term stability, we focused on the lights on bridges. The bridge lights have several advantages. First, bridges are above water, which has low reflectance and works well when used as background. Second, bridges are typically made of concrete with moderate level of reflectance in the DNB spectral range. Third, bridges are mostly illuminated at night. On the negative side, there are transient traffic lights contributing to the brightness. We assume that the contribution from the traffic is relatively constant long-term. In this study, we focus on the San Mateo bay bridge (Figure 6) which is located between San Francisco and San Jose, California, and the Incheon airport bridge in South Korea.

Figure 6. Nightlight from the San Mateo Bridge.

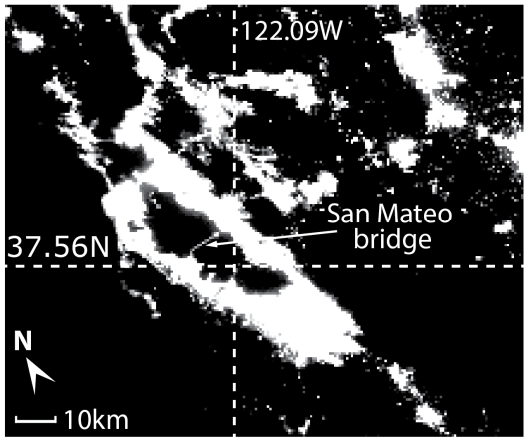

Figure 7 shows one-year pixel-level averaged radiance data over the San Mateo bridge. Several features can be seen in this time series. First, the largest spike in the time series occurred on 21 November 2013. We found that it was due to a combination of lunar illumination near fully moon and cloud cover, which has high reflection of moonlight at the time. The minimum radiance within the region (normally would be over water) is also high due to cloud cover and lunar illumination. A similar spike with a lower magnitude was found on 16 May 2014. This is likely due to a combination of two effects. There was a solar eclipse event on 29 April 2014, which contaminated the solar diffuser calibration data as well as the DNB offset data (the latter was collected during new moon around 29 April 2014). This contamination led to a positive bias in the calibration coefficients and calibrated radiances [23]. Meanwhile, on 16 May 2014, it was near full moon and the reflected lunar radiance also contributed to the up spike.

Figure 7. DNB over San Mateo bridge one-year time series with 16 day sampling interval (each data point for the radiance represents an average of 12 pixel taken along the bridge).

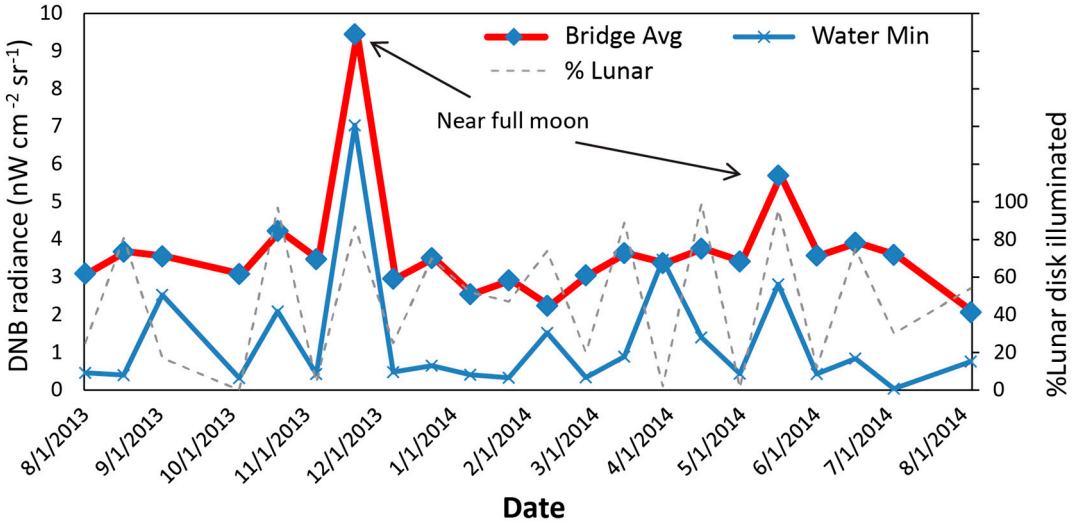

Second, other than the moon illuminated cases, the radiance values for nearly all cases are in the range of 2–4 nW·cm^{-2}·sr^{-1}. This is lower than expected as discussed later, given the density of the light poles on the bridge. Third, the radiance values have a relatively large variability between the sampled pixels, and over time as well for the same pixel. This is likely due to various factors including traffic lights which are transient. Finally, the last data point in the time series (4 August 2014) appears to have much lower values than those of the previous points. This could be due to either dark clouds or calibration uncertainties because the DNB straylight correction lookup table (LUT) was not updated promptly in the summer of 2014. However, this will require further investigation with a longer time series.

The nominal radiance for the bridge from VIIRS DNB is 3.28 nW·cm^{-2}·sr^{-1}. To validate this value, we investigated the bridge lights on the San Mateo bridge from several sources. We excluded pixels near the shore on both sides of the bridge so only ~10 km of the bridge with 12 VIIRS DNB pixels are included in the analysis. From the DNB image, it is found that the angle between cross-scan and the bridge is 32 degrees. Therefore, the bridge segment length in each pixel is actually 875 m, and each pixel has 31.9 lamps, which include both sides of the bridge with a deck width of 25.9 meters.

According to the California Department of Transportation (DOT), the light poles are 180 feet (or 54.86 meters) apart, and white LEDs have replaced the HPS lamps with equivalent power. Both LED and HPS are known to have an electrical to radiant power conversion efficacy of 30% [24]. The lamp height is known to be 30 feet or 9.144 m. Given the geometry of the lamp setup, the solid angle of each lamp that the bridge surface intercepts the light is estimated to be 1.43 sr, while the lamp is assumed radiating into a 2 π space. As shown in Table 2, the estimated DNB radiance would be 3.88 $nW \cdot cm^{-2} \cdot sr^{-1}$. This is more than 18% higher than the DNB observations. It also does not include lights contributed from the headlights of the cars and trucks on the bridge at the time (approximately 1:30 a.m., local time). We have verified all parameters used in the calculation and all results are consistently higher than the DNB observed radiances. The uncertainties in the calculations are dominated in the geometric factor and aerosol as discussed later.

Table 2. San Mateo Bridge Light Radiance Validation.

DNB OBSERVATION		
Nominal radiance (pixel level)	3.28 $nW \cdot cm^{-2} \cdot sr^{-1}$	Radiance time series
Angle between DNB crosstrack and bridge	32 degrees	Computed from DNB image
Bridge segment length within each DNB pixel at nadir	875 m	Based on 32 degree angle above and 742 m pixel size
VALIDATION		
LED Lamp Electrical Power	310 W	Per lamp on east flat segment, or 400 W for the western high rise segment; California DOT
Radiant efficacy from electrical to optical power	30%	Y. Zong, NIST
White LED % radiant power within DNB spectral range	66%	Ratio of integration from typical white LED spectra and DNB spectral response
Radiant power to hemisphere	9.77 W/sr	Uncertainties due to lack of specific details on the viewable angles
Lamp height	9.144 m	California DOT
Solid angle of illuminated area (per lamp)	1.43 sr	Computed based on lamp height, deck width, and Google map measurements; uncertainty due to actual area illuminated.
Radiant power intercepted by bridge	13.92 W	Equations (2)
Surface Lambertian reflection	18%	From AVIRIS spectral reflectance; uncertainty due to subpixel mixing at 16 m resolution.
Bridge reflected radiance per lamp	0.798 W sr^{-1}	Equations (1) and (2)
Lamp spacing	54.86 m	California DOT
#Lamps per pixel	875/54.86 × 2 = 31.9	
Radiance per DNB pixel	4.62 E−5 $W \cdot m^{-2} \cdot sr^{-1}$	Equations (1) and (2); Each pixel area 742 × 742
Atmospheric transmittance	0.84	MODTRAN plus AERONET; uncertainty due to lack of *in situ* data
Predicted DNB radiance	3.88 $nW \cdot cm^{-2} \cdot sr^{-1}$	>13% higher than the nominal radiance from DNB observations

The lights on the Incheon bridge are brighter (nominal value is 15 $nW \cdot cm^{-2} \cdot sr^{-1}$) for two reasons: (1) The spacing between lights are smaller (~15 m according google images) which leads to a higher density. (2) The lamps may have better efficacy and spectral coverage by the DNB. However, cloud is

a major issue for the Incheon bridge and as a result, the one year time series with 16 day repeating cycle has many missing data points especially in the summer month.

Despite the calculated values are not exact, the results are encouraging. First of all, the one-year time series was able to reveal DNB LUT issues as discussed earlier. Secondly, the time series can be further refined with better *in situ* information about the lights. Third, it shows that a better light source can be specifically designed for DNB calibration use by taking a few simple steps, such as increasing the reflectance of the surface or radiating upward directly, fully capturing the lights from the source to avoid light loss, and using light bulbs with better radiant efficacy and spectral range. Therefore, with a light source specifically designed for DNB calibration monitoring such as using red LEDs, the light power needed to illuminate the DNB pixel at the 3 $nW \cdot cm^{-2} \cdot sr^{-1}$ level can be significantly reduced.

In contrast to the crab fishing vessel and bridge studies, the light intensity of Geneva city is much higher as expected. The main disadvantage in analyzing city lights is that the abundant light sources can cause significant cross pixel contamination in the samples. In other words, point source analysis using city lights is very difficult. Here we analyze the pixels with the maximum light intensity within the city to see if they are stable with the assumption that the maximum values are less contaminated by nearby pixels. Table 3 shows the pixels with the maximum light intensity from selected sample dates.

Table 3. The brightest pixels in Geneva city.

Dataset	Lat/Lon of the pixel	Radiance
20140606_t0144510	46.222590/6.134870	383.677 $nW \cdot cm^{-2} \cdot sr^{-1}$
20140521_t0140214	46.222599/6.142890	279.319 $nW \cdot cm^{-2} \cdot sr^{-1}$
20140419_t0142441	46.223026/6.135354	504.672 $nW \cdot cm^{-2} \cdot sr^{-1}$
20140318_t0139254	46.2194791/6.140902	299.144 $nW \cdot cm^{-2} \cdot sr^{-1}$
20140313_t0135527	46.221821/6.137994	189.686 $nW \cdot cm^{-2} \cdot sr^{-1}$

Several phenomena are observed from the brightest light pixels in the Geneva city. First, the brightest pixels are mostly located in the Paquis Nation area along the Ave. De France, which is not too far from the World Meteorological Organization, as well as the IPCC (International Panel for Climate Change). Second, the brightest spots have typical values of greater than 180 $nW \cdot cm^{-2} \cdot sr^{-1}$. However, the brightest pixels are not always found in the same pixel location. For example, the 5 May 2014 dataset had the brightest point on the north side near the train station, while 16 days later, the brightest spot was found further south, and with a much different radiance value. The changing location of the brightest pixels can be due to several possibilities such as small geo-location differences in the pixel location between observations, but in any case the lights are not stable and may not be suitable for stability analysis intended for this study. This also suggests that the DNB spatial resolution is a limiting factor for urban light analysis. The DNB resolution can potentially be enhanced since inherently the DNB has higher spatial resolution at subpixel level before the aggregation [10].

The alternative to city nightlight point source analysis is apparently using averaged city lights over a large geographic region such as the entire city. This type of analysis has been done in previous studies, which showed potentials [25]. However, the issue with averaged light power for a region is that the absolute power calculated would be very difficult to validate. Additionally, as more efficient light bulbs are replacing the traditional types, this may introduce more uncertainties for regional

analysis due to the mixing of light bulb types. This is also part of the reason that this study focuses on point source analysis.

4.2. Atmospheric Effects

To estimate the atmospheric effects, we used MODTRAN to perform calculations for various water vapor and aerosol amount. The US standard atmosphere is used as a baseline, while the water vapor was scaled from 0.1 to 1.0 in the calculations, and 10 types of aerosols were used. The results show that the water vapor variability has a small effect on the light transmittance of the DNB band. The variability between dry and wet atmospheres on transmittance is on the order of 1.8%. Note that the DNB has a spectral response cutoff at 0.9 μm, which is just before the major water vapor absorption at 0.94 μm.

On the other hand, the aerosol type has a major impact on the transmittance. Figure 8 shows that with no aerosols, the transmittance is at ~0.9, while with 5 km visibility, the transmittance is at 0.4. Maritime aerosol has a moderate impact with a transmittance about 0.7, and urban aerosols can have transmittance as low as 0.4. Since the San Mateo bridge is in-between cities and over water, we choose to use a transmittance of 84% for the calculations earlier. Further verification using AERONET data at the nearby Monterey station suggests that this value is reasonable.

Figure 8. VIIRS DNB Transmittance variations with aerosol types (Transmittance = 1 − Extinction).

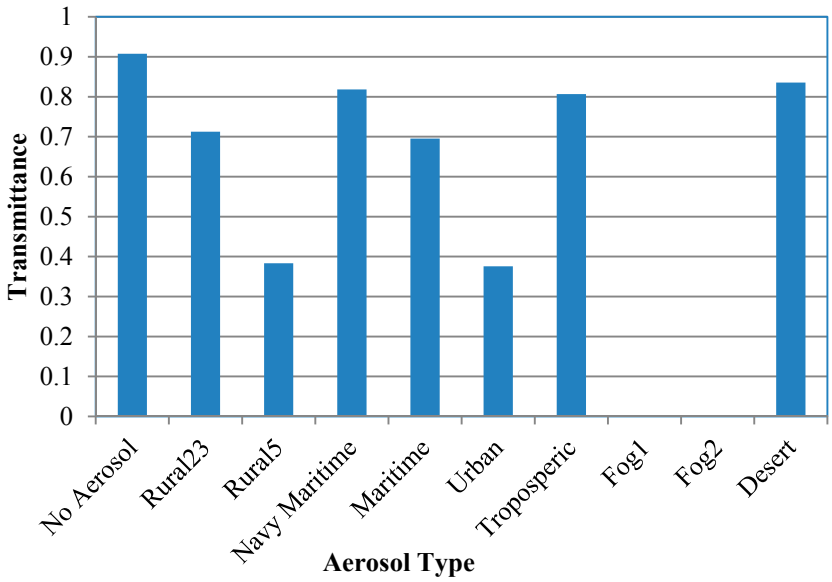

As discussed in the methodology section, since none of the radiative transfer models currently allows input of active light source, the calculations in this study are only for transmittance of water vapor and aerosols. Scattering effect is not included in this analysis.

4.3. Uncertainty Reduction

Based on the analysis in previous sections, it is clear that the nightlight point sources can potentially be good targets for the validation of DNB calibration stability and absolute accuracy at low radiances. The primary uncertainty in estimating the light power of point sources from the VIIRS DNB, and estimating the stability of the nightlights is the lack of sufficient ground truth. In the case of the fishing vessel, neither the deck surface reflectance nor the light bulb type is known which contributes to uncertainties in the calculations. Similar issues exist for the bridges, where the geometric factors require specific details such as lamp view angle and illuminated area on the bridge. In general, calculating radiometric quantities based on electrical power may not be reliable. *In situ* radiance measurement is essential in reducing the uncertainties. In addition, the effect of transient traffic lights is not included, and aerosols were not measured onsite.

Currently, it is difficult to separate the stability of the light source from the stability of the VIIRS DNB calibration. Atmospheric effects are simulated only partially (transmittance only), since currently models cannot incorporate artificial light source. The effect of scattering loss from aerosols, which has not been accounted for in this study, can be significant for nightlight point sources and may partially explain the low biases in the DNB observations. Finally, there are many other potential factors that could affect the uncertainties in the calculations, including but not limited to, residual straylight effects in the correction of DNB, air glow, and others.

These uncertainties raise the question about the accuracy that existing active light sources will allow us to achieve. It also points to the need for more accurate low light sources specifically designed for such purposes. This study shows that given the high sensitivity of the VIIRS DNB, it is quite feasible to design and install light sources which are well controlled and the accuracy well quantified. Our study shows that the light power required does not have to be high, depending on the type of light bulbs used. Good candidates include the latest power LEDs, which are known to be stable with low electrical power requirements. Red LEDs would be preferred over white LEDs for DNB due to its spectral range and better efficacy. Tungsten lamps have high electrical to radiant power efficacy and can also be an alternative.

Therefore, this study also serves as an initial assessment of the need and feasibility for developing an accurate active light source for VIIRS DNB calibration. Such a system would not only improve the low light calibration accuracy, but also the point spread function, as well as geolocation accuracy at night. This will potentially significantly improve the calibration accuracy and stability of the VIIRS DNB, which in turn will allow us to estimate environmental changes such as atmospheric variability as in aerosol retrievals at night, and potentially enable many other applications. *In situ* knowledge of the lamps and radiance measurements are essential to reduce uncertainties.

5. Conclusions

This study demonstrates for the first time that the VIIRS DNB radiances from point sources such as those from fishing vessels, bridges, and city light bulbs at radiance levels near 3 $nW \cdot cm^{-2} \cdot sr^{-1}$ can potentially be used to estimate relatively accurately the electrical power used based first principle physics. Our analysis of the radiant power using fundamental radiometry, point cloud analysis, and

radiative transfer models enables the quantitative assessment of the light power used, although the uncertainties can be greater than 13% largely due to lack of ground truth. Time series analysis of light power on the bridges in this study has shown potential to reveal VIIRS DNB calibration stability at low radiances, as well as the stability of the light sources. It was found that the VIIRS DNB at the specified minimum radiance (L_{min} of 3 $nW \cdot cm^{-2} \cdot sr^{-1}$) has strong signal to noise ratio and can be used for a variety of application for point source objects if the instrument is accurately calibrated. On the other hand, the incomplete ground truth data and lack of suitable radiative transfer models for nightlight point source calculations dominates the uncertainties in the analysis. The way forward is to reduce the uncertainties by developing accurate active light sources (preferably SI traceable) specifically designed for the VIIRS DNB nighttime monitoring. Such a system will not only enable more accurate radiometric, geolocation, and point spread function characterizations and monitoring of the DNB, but potentially can enable more novel environmental monitoring applications such as nighttime aerosol retrievals.

Acknowledgements

We would like to thank Yuqin (Eugene) Zong of NIST for fruitful discussions on possible active light sources and his help in clarifying the efficacy of light bulb types. We also thank Parviz Boozarpour and colleagues, from the district 4, California Department of Transportation (DOT), for providing detailed information about the light bulbs and setup on the San Mateo bridge. Thanks are extended to Xi Shao for providing information on LPTRAN and Garstang models, and Slawirmir Blonski (both from the University of Maryland) for clarifying the DNB performance and operational issues. This study is partially funded by the JPSS program. The manuscript contents are solely the opinions of the author(s) and do not constitute a statement of policy, decision, or position on behalf of NOAA or the U.S. Government.

Author Contributions

Changyong Cao conceived and designed the study, analyzed the data, and wrote the paper; Yan Bai supported the study with data acquisition, processing, and analysis, as well as graphic drawing.

Conflicts of Interest

The authors declare no conflict of interest.

References

1. Miller, S.; Straka, W.; Mills, S.; Elvidge, C.; Lee, T.; Solbrig, J.; Walther, A.; Heidinger, A.; Weiss, S. Illuminating the capabilities of the Suomi National Polar-Orbiting Partnership (NPP) Visible Infrared Imaging Radiometer Suite (VIIRS) day/night band. *Remote Sens*. **2013**, *5*, 6717–6766.
2. Liang, C.K.; Mills, S.; Hauss, B.I.; Miller, S.D. Improved VIIRS day/night band imagery with near-constant contrast. *IEEE Trans. Geosci. Remote Sens*. **2014**, *52*, 6964–6971.
3. Liao, L.; Weiss, S.; Mills, S.; Hauss, B. Suomi NPP VIIRS day-night band on-orbit performance. *J. Geophys. Res*. **2013**, *118*, 12705–12718.

4. Cao, C.; Xiong, J.; Blonski, S.; Liu, Q.; Uprety, S.; Shao, X.; Bai, Y.; Weng, F. Suomi NPP VIIRS sensor data record verification, validation, and long-term performance monitoring. *J. Geophys. Res*. **2013**, doi:10.1002/2013JD020418.
5. Cao, C.; Shao, X.; Uprety, S. Detecting light outages after severe storms using the Suomi-NPP/VIIRS day night band radiances. *IEEE Geosci. Remote Sens. Lett.* **2013**, *10*, 1582–1586.
6. VIIRS DNB Cloud Free Composites. Available online: http://ngdc.noaa.gov/eog/viirs/download_monthly.html (accessed on 20 November 2014).
7. Elvidge, C. NOAA/NGDC, Boulder, CO, USA. Personal communication, 2014.
8. Steradian. Available online: http://en.wikipedia.org/wiki/Steradian (accessed on 20 November 2014).
9. Lin, G. NASA/VIIRS Characterization Support Team, Greenbelt, MD, USA. Personal communication, 2014.
10. McCarthy, J.; Jacobson, E.; Kilduff, T.; Estes, R.; Levine, P.; Mills, S.; Elvidge, C.; Miller, S. On the potential to enhance the spatial resolution of the day/night band (DNB) channel of the visible and infrared imaging radiometer suite (VIIRS) for the second joint polar satellite system (JPSS-2) and beyond. In Proceeding of 2013 Earth Observing Systems XVIII, San Diego, CA, USA, 23 September 2013.
11. CloudCompare. Available online: http://en.wikipedia.org/wiki/CloudCompare (accessed on 20 November 2014).
12. Garstang, R.H. Night-sky brightness at observatories and sites. *Publ. Astron. Soc. Pac*. **1989**, *101*, 306–329.
13. Shirkey, R.C. An Army Illumination Model (AAIM). Available online: http://www.arl.army.mil/arlreports/2008/ARL-TR-4645.pdf (accessed on 20 November 2014).
14. Cinzano, P.; Falchi, F.; Elvidge, C. Recent Progresses on a Second World Atlas of the Night-Sky Brightness Lptran/Lpdart Realistic Models, Tomography of Light Pollution, Accurate Validation Methods and Extended Satellite Data Analysis, Starlight: A Common Heritage. Available online: http://www.starlight2007.net/prolightpollution.htm (accessed on 20 November 2014).
15. Berk, A.; Bernstein, L.S.; Anderson, G.P.; Acharya, P.K.; Robertson, D.C.; Chetwynd, J.H.; Adler-Golden, S.M. MODTRAN cloud and multiple scattering upgrades with application to AVIRIS. *Remote Sens. Environ.* **1998**, *65*, 367–375.
16. Vermote, E.; Tanre, D.; Deuze, J.L.; Herman, M.; Morcrette, J. Second simulation of the satellite signal in the solar spectrum, 6S: An overview. *IEEE Trans. Geosci. Remote Sens.* **1997**, *35*, 675–686.
17. CRTM. Available online: http://en.wikipedia.org/wiki/Community_Radiative_Transfer_Model (accessed on 20 November 2014).
18. Han, Y.; Delst, P.; Liu, Q.; Weng, F.; Yan, B.; Derber, J. CRTM User's Guide. Available online: http://www.star.nesdis.noaa.gov/smcd/spb/CRTM/crtm-code/CRTM_UserGuide-beta.pdf (accessed on 20 November 2014).
19. Henrich, T.; Fisher, W.; Broderson, D.; Cable, J.; Macfarlane, S.; Stevens, E.; Cole, K. Legatt, R. Available online: http://www.testbeds.noaa.gov/events/2014/workshop/presentations/posters/Heinrichs_Real-time-GIS-Satellite-Data-Feeds-to-NWS-Alaska-Sea-Ice-Program-Heinrichs-etal-TBPG-workshop-April-2014-1.pdf (accessed on 20 November 2014).

20. Global Gridded NPP, AQUA and TERRA Images. Available online: http://peate.ssec.wisc.edu/flo/npp/gridding (accessed 20 November 2014).
21. Heidinger, A. NOAA/NESDIS/STAR, Madison, WI, USA. Personal communication, 2014.
22. Elvidge, C.; Keith, D.; Tuttle, B.; Baugh, K. Spectral identification of lighting type and character. *Sensors* **2010**, *10*, 3961–3988.
23. Lee, S. NASA/VIIRS Characterization Support Team, Greenbelt, MD, USA. Personal communication, 2014.
24. Zong, Y. NIST, Gaithersburg, MD, USA. Personal communication, 2014.
25. Uprety, S. Cooperative Institute for Research in the Atmosphere, Colorado State University, Fort Collins, CO, USA. Personal communication, 2014.